

Linear and nonlinear topology optimization of origami structures based on crease pattern and axial rigidity

Original

Linear and nonlinear topology optimization of origami structures based on crease pattern and axial rigidity / Cretella, Vincenzo; Sohouli, Abdolrasoul; Pagani, Alfonso; Suleman, Afzal. - In: STRUCTURAL AND MULTIDISCIPLINARY OPTIMIZATION. - ISSN 1615-147X. - 67:5(2024). [10.1007/s00158-024-03773-3]

Availability:

This version is available at: 11583/2989573 since: 2024-06-17T08:52:53Z

Publisher:

SPRINGER

Published

DOI:10.1007/s00158-024-03773-3

Terms of use:

This article is made available under terms and conditions as specified in the corresponding bibliographic description in the repository

Publisher copyright

(Article begins on next page)

Linear and Nonlinear Topology Optimization of Origami Structures based on Crease Pattern and Axial Rigidity

Vincenzo Cretella^{1,2}, Abdolrasoul Sohoul³, Alfonso Pagani²,
Afzal Suleman^{2,3*}

¹Department of Mechanical and Aerospace Engineering, Politecnico di Torino, Corso Duca degli Abruzzi 24, Turin, 10129, Italy.

^{2*}IDMEC, Institute of Mechanical Engineering, Instituto Superior Técnico, Universidade de Lisboa, Av. Rovisco Pais, No. 1, Lisbon, 1049-001, Portugal.

^{3*}Department of Mechanical Engineering, Center for Aerospace Research, University of Victoria, 3800 Finnerty Rd, Victoria, V8W 2Y2, British Columbia, Canada.

*Corresponding author(s). E-mail(s): suleman@uvic.ca;
Contributing authors: vincenzo.cretella@tecnico.ulisboa.pt;
sohouli@uvic.ca; alfonso.pagani@polito.it;

Abstract

Origami structures exhibit desirable stowage properties for application in deployable space structures. This work aims to improve a design methodology for origami structures using topology optimization of truss models. The objective is to find the optimal configuration of the truss structure based on axial rigidity and the crease pattern that maximizes the displacement at set locations, under prescribed forces and boundary conditions. First, a linear method is used to determine small strains and small rotations to evaluate the performance at the initiation of folding. Subsequently, a nonlinear method is implemented to consider large displacements and large rotations. To carry out the optimization process, constraints on the number of active fold lines and on the axial rigidity distribution are applied. Previous studies on topology optimization of origami structures have focused on folding and bending in their analyses. Here, it is shown that including axial rigidity as a design variable leads to new and promising origami designs.

1 Introduction

Origami is the ancient Japanese art of paper folding that has deep roots and its own philosophy. In the seventies, some researchers discovered that in theory, through conventional origami, an infinite number of shapes could be obtained. This enabled new applications, allowing the discovery of new promising designs for many engineering structures.

The reason why origami are so versatile, especially in the aerospace field, is that it takes a two-dimensional component (like a plate) into a three-dimensional one. Moreover, space structures must be lightweight and compact during launch, while being deployable in space to maximize the surface area. Therefore, the most relevant applications of space origami are deployable space arrays and antennas [1–4]. To this end, it is necessary to develop models and analysis methods to allow for the understanding and computational implementation of their kinematics and mechanics. Such a task is quite complex because of the intricate designs and folding motions of these structures.

At the foundation of every origami design approach, there are many theoretical notions to consider such as the definition of folds and the fold constraints [5, 6]. Numerous studies have considered rigidly foldable fold patterns [7] and various kinematic approaches have been applied [6–8], using the assumptions that the facets are rigid and do not bend nor stretch and that the folds are creases (i.e. straight lines with zeroth-order geometric continuity). To improve on this analysis, Schenk et al. [9] introduced a truss model to allow for facet deformations using a linear method, hence considering only small strains and small deformations. The truss model simplifies the configuration of the origami: each vertex in the folded sheet is represented by a pin-joint and every border and fold line by a truss element. This method was applied to topology optimization by Fuchi et al. [10, 11] to discover origami crease patterns that maximize displacements at set locations.

To take into account the large deformations and large rotations typical of origami, nonlinear models are required. Filipov et al. [12] and Liu et al. [13] introduced a truss and hinge model to consider material and geometric nonlinearities. Also, Filipov et al. [14] validated the accuracy of these truss models by comparing them to shell and 3D continuum elements. A nonlinear truss model was introduced by Gillman et al. [15], based on the positional finite element truss proposed by Greco et al. [16], considering a torsional spring around each truss element of the origami. There, periodic boundary conditions were described to analyze origami tessellation patterns.

Origami structures exhibit one or more critical points during their folding motions, therefore the arc-length method, first introduced by Risks [17, 18] and Wempner [19], and later analyzed by Leon et al. [20], was included in the formulation by Gillman et al. [15]. Also, the Modified Generalized Displacement Control Method (MGDCM) as introduced by Leon et al. [21] was employed to find efficient solutions for the system of nonlinear equations while adjusting the step size based on the loading profile curvature.

Lastly, modal analysis is required to distinguish and follow the multiple bifurcation branches off the flat state typical of origami structures with complex designs. To consider this bifurcation problem, Tachi and Hull [22] focused on fully rigid facets, while Santangelo [23] neglected fold stiffness, considering only fold stretching. Therefore, Gillman et al. [15] introduced a formulation to consider both fold stiffness and fold stretching in modal analysis.

The modified nonlinear truss model by Gillman et al. [15] was later applied to topology optimization [24, 25], however employing a simple Newton-Raphson method to solve the system of nonlinear equations introduced by the problem. There, a procedure to find an origami crease pattern that achieves the desired large deformation through folding for a given input force was provided, using the fold stiffness as a design variable and applying a constraint on the number of fold lines.

Lastly, Gillman et al. [26] applied the topology optimization method with the truss model to discover origami structures with auxetic behavior, like the Miura-Ori fold pattern [27].

The main objective of this work is to improve the topology optimization method proposed by Fuchi et al. [11] regarding linear analysis and by Gillman et al. [25] regarding nonlinear analysis, introducing axial rigidity as a design variable thus allowing each truss to stretch in an optimized way. Although the complexity of the problem is slightly increased with respect to these works, this modification enables to obtain new promising origami designs.

Gillman et al. [24, 25] applied both gradient and non-gradient-based methods to topology optimization, making comparisons between the different obtained results. Here, to emphasize convergence speed, two gradient-based methods are used to perform the optimization: the Method of Moving Asymptotes (MMA) [28] and the Sequential Quadratic Programming (SQP) [29]. Also, the axial rigidity distribution is optimized through the modified Solid Isotropic Material with Penalization (SIMP) method presented by Andreassen et al. [30].

2 Topology Optimization based on Linear Analysis

In this Section, a linear truss method is used to study small displacements and small rotations in flexible origami structures. Fig. 1 shows a general starting configuration of origami with this method. Each fold line and external segment in the sheet (grey lines in Fig. 1) is represented by a truss element, while each vertex, i.e. each node in the starting configuration (black points in Fig. 1) is represented by a pin-joint.

Following the method introduced by Schenk and Guest [31], modeling the folding patterns as a pin-jointed framework allows the use of established structural engineering methods to study the mechanics of origami. The mechanical properties of the Reference grid are described by introducing a stiffness formulation, that relates the nodal displacements \mathbf{u} with the applied nodal forces \mathbf{F} through the material stiffness matrix \mathbf{K} :

$$\mathbf{K}\mathbf{u} = \mathbf{F}. \quad (1)$$

The matrix \mathbf{K} can be obtained from:

$$\mathbf{K} = \mathbf{K}_J + \mathbf{K}_T, \quad (2)$$

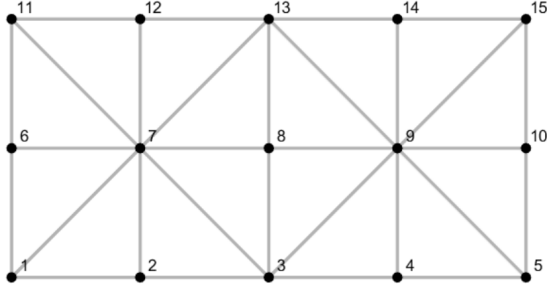


Fig. 1: Reference grid of an origami sheet in the linear truss method.

where \mathbf{K}_J and \mathbf{K}_T are the stiffness matrices obtained from the fold constraint [5] and the truss model respectively.

In this Section, a *linear analysis* will be carried out, i.e. the stiffness matrix remains constant and independent of \mathbf{u} during the formulation. This has the advantage of having a low computational cost, but the drawback is that the applied loads are required to be small, leading to small deformations. Also, this analysis cannot be used in origami designs that involve a sequence of folding with altering overall directions of deformation. Even though origami folds usually generate large deformation, this analysis can determine the optimal topology for the initiation of folding.

2.1 Optimization Methods

2.1.1 Fold Constraint

The folding mechanism is derived from constraints on the relationship between the dihedral angles (ϕ) and the nodal coordinates (\mathbf{X}):

$$\mathbf{J} = \frac{d\phi}{d\mathbf{X}}. \quad (3)$$

This Jacobian can be evaluated considering each dihedral angle ϕ relative to adjacent facets, like in Fig. 2, that is:

$$\phi = \sin^{-1} \left[\frac{\mathbf{v}_{12} \times (\mathbf{v}_{14} \times \mathbf{v}_{12}) \cdot (\mathbf{v}_{12} \times \mathbf{v}_{13'})}{\sin \gamma \sin \beta \|\mathbf{v}_{12}\|^3 \|\mathbf{v}_{13'}\| \|\mathbf{v}_{14}\|} \right] \quad (4)$$

where \mathbf{v}_{ij} is the vector from node i to j .

For each fold line k , the fold stiffness K_J^k can be computed as:

$$K_J^k = (J^k)^T G_k J^k, \quad (5)$$

where $k = 1, \dots, N_f$, N_f is the number of fold lines and G_k is the fold stiffness relative to folding, hence it is equal to zero in the trusses at the boundaries. By changing this coefficient, it is possible to regulate the importance of the fold constraint along each

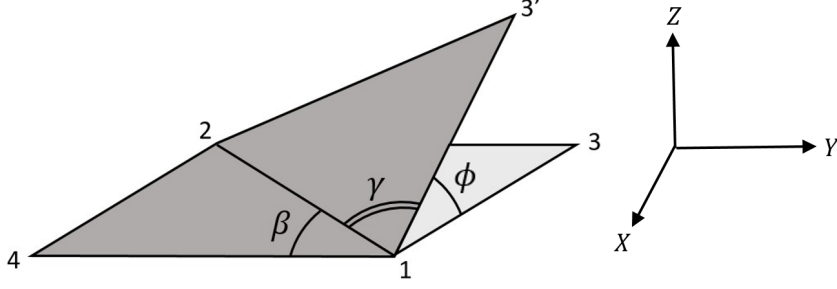


Fig. 2: Scheme of the origami element in the linear truss model.

fold line k : folding is allowed using a small G_k (G_{soft}), while it is prevented using a large G_k (G_{stiff}).

Fuchi et al. [11] proposed a design method for origami structures using topology optimization considering the fold stiffness G as a design element, to discover the *optimized crease pattern*, i.e. the configuration of fold lines in the origami that allows to achieve the greatest actuation. Only the fold lines required to obtain this actuation are revealed after the analysis, considering a constraint on the maximum allowable number of fold lines that can be active (i.e. soft folds with small values of G that allow folding), hiding the remaining inactive fold lines (i.e. stiff folds with large values of G that do not allow folding). The fold stiffness is represented by the following function

$$G_k = 10^{a_0 + \alpha_k(a_1 - a_0)}, \quad (6)$$

which is continuous and differentiable to allow to use gradient-based optimization algorithms. The design variable $\alpha_k \in [0, 1]$ (i.e. the fold stiffness exponent associated with folding) is considered, while a_0 and a_1 are constants and G_k takes on values from $G_{soft} = 10^{a_0}$ to $G_{stiff} = 10^{a_1}$.

2.1.2 Truss Model including Axial Rigidity as Design Variable

The stiffness matrix from the truss model is the sum of every elemental stiffness matrix of the truss elements k_e^j , as follows:

$$\mathbf{K}_T = \sum_{j=1}^{N_e} k_e^j, \quad (7)$$

where k_e^j is a function of the axial rigidity EA_j ($j = 1, \dots, N_e$) and N_e is the number of truss elements.

In this Chapter, the optimization method introduced by Fuchi et al. [11] is improved to consider also the axial rigidity EA as a design variable, discovering both the optimized crease pattern and the *axial rigidity distribution*, i.e. the origami configuration in terms of the axial rigidity of each truss that allows to achieve the greatest actuation. To obtain the axial rigidity, a density-based approach to topology optimization can be considered, similar to the modified SIMP approach applied by Andreassen

et al. [30]. The design domain is discretized by finite elements with an assigned axial rigidity density β :

$$EA_j = EA_{min} + \beta_j^p (EA_0 - EA_{min}), \quad (8)$$

where N_e is the number of truss elements, EA_0 the axial solid rigidity of the material (or maximum axial rigidity), EA_{min} the axial void rigidity (or minimum axial rigidity) assigned to avoid singularity and p a penalization factor that ensures black-and-white solutions.

The difference between this approach and the one used by Andreassen et al. [30] is that the axial rigidity (EA) is chosen as the design variable instead of the Young's Modulus (E). This procedure leads to manufacturing advantages of the trusses in the structure since it is possible to either alter the size or the material of the trusses during fabrication. Today's additive manufacturing techniques, known as *Multi-Material Additive Manufacturing* (MMAM), are capable of using various materials and allow for the deposition of multiple materials in a single print job [32]. These techniques also allow for the achievement of desirable properties by utilizing the concept of gradient lattice structures. As a result, it is possible to tailor the axial rigidity, which significantly increases the design space.

Lastly, in the non-modified SIMP approach [33, 34], elements with zero stiffness are avoided by imposing a limit value on the densities β . In this method, this is done by the factor EA_{min} , which allows for a more straightforward implementation.

2.2 Optimization Framework

The aim of this optimization is to find the axial rigidity distribution of the trusses and the origami crease pattern that maximizes the displacement at set locations, achieving the desired deformations through folding and stretching for a given input force.

The *optimization problem* is the following:

<p>Find $\mathbf{x} = \alpha_1, \dots, \alpha_{N_f}, \beta_1, \dots, \beta_{N_e}$ that</p> <p>Minimize $f = -\mathbf{c}^T \mathbf{u}$</p> <p>Subject to</p> $g_1 = v_{0,1} - \frac{1}{N_f} \sum_{i=1}^{N_f} x_i \leq 0; \quad g_2 = v_{0,2} - \frac{1}{N_e} \sum_{i=N_f+1}^{N_f+N_e} x_i \leq 0; \quad (9)$ $0 \leq x_i \leq 1; \quad \forall i = 1, \dots, N_f + N_e;$ <p style="text-align: center;">Ku = F.</p>

f is the objective function, hence minimizing f means maximizing the displacements along a direction, where \mathbf{c} is a vector that selects the displacements relative to the problem, taking on values of either 1, -1 or 0 to indicate the associated direction of optimal actuation. $g_1 \leq 0$ and $g_2 \leq 0$ are the two inequality constraints:

- g_1 limits the number of foldlines to meet design requirements given a total of N_f available lines, while $v_{0,1}$ limits the fold stiffness used in the structure.
- g_2 limits the number of trusses that are allowed to have an axial solid rigidity EA_0 to meet design requirements given a total of N_e available lines, while $v_{0,2}$ limits the axial rigidity used in the structure.

The objective function varies according to two parameters:

- $l_0 = 1 - v_{0,1}$: constraint on the number of active fold lines allowed. If $l_0 = 0$ no fold line of the starting configuration is active, while if $l_0 = 1$ all the fold lines are active;
- $m_0 = 1 - v_{0,2}$: constraint on the number of trusses that are allowed to have a minimum axial rigidity. If $m_0 = 0$ every truss member has axial rigidity $EA = EA_0$, while if $m_0 = 1$ every truss member has axial rigidity $EA = EA_{min}$.

The value of the design variables is limited to take on values between 0 and 1 from the second constraint. The final constraint is the governing equation of the system.

An overview of the algorithm is shown in Fig. 3.

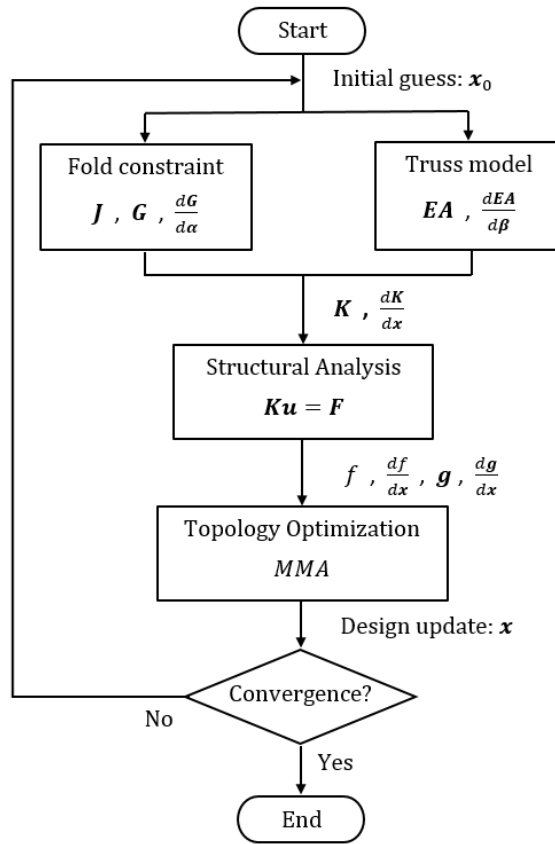


Fig. 3: Flow chart of the linear optimization process.

2.2.1 Sensitivity analysis

To use the aforementioned gradient-based algorithms, a sensitivity analysis needs to be carried out, therefore the derivative of the objective function with respect to the design variables needs to be computed.

The addition of the second set of design variables implies the use of two constraint functions (g_1 and g_2), as shown in the Optimization Framework (9), that are assembled in a vector

$$\mathbf{g} = [g_1; g_2]. \quad (10)$$

However, a gradient-based optimization also needs the gradient of the constraint function with respect to the design variables

$$\frac{d\mathbf{g}}{d\mathbf{x}} = \begin{bmatrix} \frac{dg_1}{d\mathbf{x}} & \frac{dg_2}{d\mathbf{x}} \end{bmatrix}, \quad (11)$$

which is a matrix containing two vectors with the same length of \mathbf{x} .

The derivative of the stiffness matrix is found as:

$$\frac{\partial \mathbf{K}}{\partial \mathbf{x}} = \frac{\partial \mathbf{K}_J}{\partial \boldsymbol{\alpha}} + \frac{\partial \mathbf{K}_T}{\partial \boldsymbol{\beta}}, \quad (12)$$

where $\boldsymbol{\alpha} = x_1, \dots, x_{N_f}$ and $\boldsymbol{\beta} = x_{N_f+1}, \dots, x_{N_f+N_e}$. The first term in Eq. (12) comes from the fold constraint

$$\frac{\partial \mathbf{K}_J}{\partial \alpha_k} = \mathbf{J}^T \frac{\partial G_k}{\partial \alpha_k} \mathbf{J} = \mathbf{J}^T \left[(a_1 - a_0) 10^{a_0 + \alpha_k (a_1 - a_0)} \log(10) \right] \mathbf{J}, \quad (13)$$

while the second one from the truss model, using a chain rule

$$\frac{\partial \mathbf{K}_T}{\partial \beta_j} = \frac{\partial \mathbf{K}_T}{\partial EA_j} \frac{\partial EA_j}{\partial \beta_j}. \quad (14)$$

In Eq. (14), $\partial \mathbf{K}_T / \partial EA_j$ is obtained from the gradient of the elemental stiffness matrix of the truss elements and

$$\frac{\partial EA_j}{\partial \beta_j} = p \beta_j^{(p-1)} (EA_0 - EA_{min}). \quad (15)$$

The gradient is obtained from the following adjoint method:

$$\mathbf{K} \begin{pmatrix} \partial \mathbf{u} \\ \partial x_i \end{pmatrix} = - \begin{pmatrix} \partial \mathbf{K} \\ \partial x_i \end{pmatrix} \mathbf{u}. \quad (16)$$

Solving Eq. (16) with \mathbf{u} and \mathbf{K} obtained from Eq.s (1) and (2) respectively, $\partial\mathbf{u}/\partial x_i$ is found, and the gradients df/dx_i can be computed as:

$$\frac{df}{dx_i} = - \left(\frac{\partial\mathbf{u}}{\partial x_i} \right)^T \mathbf{c}. \quad (17)$$

Lastly, the optimization problem can be solved using the Method of Moving Asymptotes (MMA). The whole process, schematized in Fig. 3, is described here:

1. At the start of each iteration, \mathbf{G} and \mathbf{EA} along with their gradients, are computed from the fold constraint and the truss model respectively, in order to evaluate the stiffness matrix \mathbf{K} and its gradient from Eq.s (2) and (12).
2. Through Eq. (1), the structural analysis is carried out with the purpose of finding the nodal displacement field \mathbf{u} , while its gradient is obtained from Eq. (16);
3. The objective function and its gradient from Eq.s (9) and (17) are computed, as well as the constraint functions and their gradients;
4. The gradient-based topology optimization is carried out with the MMA method, in order to obtain the design variables x_i for the next iteration;
5. This iterative process is repeated until convergence is reached, i.e. the relative error between the objective functions at the current and at the previous iteration is lower than a set tolerance.

2.3 Numerical Examples

The capabilities of the described method are shown through two different starting configurations, each of which is composed of truss members. In these examples, the stiffness coefficients are set to $a_0 = 2$ and $a_1 = 6$. Moreover, the applied forces must be small enough to remain in a linear regime, thus obtaining displacements within a 10% range of the length of the structure.

Each case is studied first using the Origami Mechanism Topology Optimizer (OMTO) in Reference [35] that uses only the fold stiffness exponent (α) as design variable and the constraint on the number of active fold lines allowed (l_0), then with a modified OMTO, which uses the method described in this Section, that also considers the axial rigidity density (β) as design variable and the constraint on the number of trusses that are allowed to have a minimum axial rigidity (m_0). However, when $m_0 = 0$ (or sufficiently close to 0 to avoid matrix singularities), the axial rigidity is kept equal among each truss, hence the second set of design variables is not considered and the same results as using only one set of design variables are obtained.

Lastly, the dashed and dotted-dashed lines in the optimized crease pattern indicate the mountain and valley folds of the origami, while the black and magenta lines in the optimized axial rigidity distribution indicate that the truss members have an axial rigidity $EA = EA_0$ or $EA = EA_{min}$ respectively.

2.3.1 Zigzag Structure

The first example considers an already folded zigzag structure. The problem has 48 design variables ($N_f = 18$ relative to α , $N_e = 30$ relative to β). The starting configuration, with the trusses distributed as in Fig. 4a, is already folded around the second, third and fourth vertical lines as in Fig. 4b. The green triangles are the fixed nodes, the red squares are the applied loads \mathbf{F} and the blue dots are the nodes where the displacements \mathbf{u} need to be evaluated.

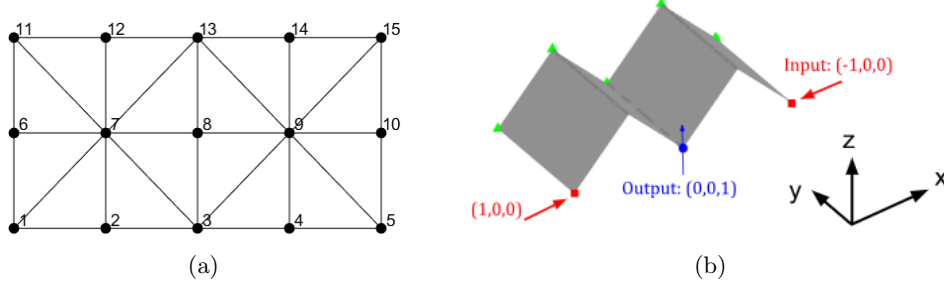


Fig. 4: Starting configuration of the zigzag structure. (a) Reference grid; (b) Load and boundary conditions ($L_x = 2.0 \text{ m}$, $L_y = 1.0 \text{ m}$, $F = 250 \text{ N}$).

The load and boundary conditions in Fig. 4b are chosen so that folding can be neglected in the small displacement analysis, in order to emphasize the stretching of the trusses. Therefore, using only α as design variable ($m_0 = 0$) it is not possible to reach convergence.

Nevertheless, keeping l_0 constant and equal for example to 0.50 and increasing m_0 the axial rigidity EA is allowed to vary among the trusses, therefore the effect of the addition of the second set of design variables can be assessed.

Considering values of m_0 from 0.10 to 0.50, new optimized configurations can be analyzed, as shown in Tab. 1. Higher values of l_0 and m_0 are not recommended since they can lead to nonlinearities and uncertain results. Usually, the desired deformation is obtained with small l_0 and m_0 .

These results underline the potential of the method. Even if the optimization problem described in this Section is more complex than the one in Reference [11], using also the axial rigidity as a design variable it is now possible to explore new configurations.

Tab. 1 displays that, if m_0 is increased, more trusses are allowed to have an axial rigidity $EA = EA_{min} = 10^4 \text{ Pa} \cdot \text{m}^2$, thus leading to a more flexible structure that can sustain larger displacements but with more design complexity and iteration steps, as shown in Fig. 5. It is also interesting to notice that, since the load condition and l_0 are kept constant during this analysis, the optimized crease pattern is the same for the considered material fractions. However, in some cases, different optimized crease patterns are obtained for the same l_0 increasing m_0 due to the modified behavior of the more flexible structure.

l_0 [-]	m_0 [-]	Optimized Crease Pattern	Axial Rigidity distribution	f [mm]
1 set of design variables (a)				
0.50	0	NO CONVERGENCE	NO CONVERGENCE	/
2 sets of design variables (a, β)				
0.50	0.10			- 40.60
	0.20			
	0.30			
0.50	0.40			- 82.50
	0.50			

Table 1: Final configurations of the zigzag structure. Dashed lines in Optimized Crease Pattern: active folds with $G = G_{soft} = 10^2 Pa \cdot m^2$. Magenta and black lines in Axial Rigidity Distribution: $EA = EA_{min} = 10^4 Pa \cdot m^2$ and $EA = EA_0 = 10^8 Pa \cdot m^2$.

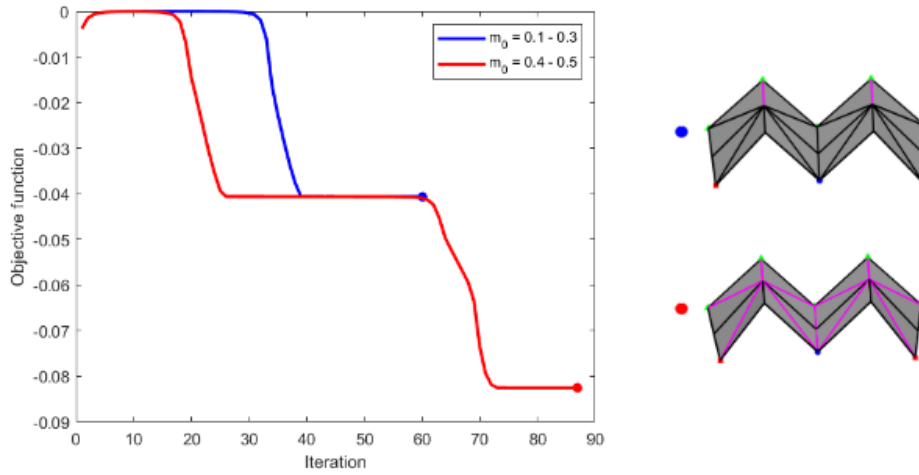


Fig. 5: Objective function over iteration for different m_0 ($l_0 = 0.5$).

2.3.2 Miura-Ori Fold Pattern

The following example is chosen to explore both the folding and stretching phenomena. The trusses in the starting configuration are displayed in Fig. 6a, and the sheet is folded like in Fig. 6b. This configuration is called *Miura-Ori*, a famous fold pattern for deployable space structures. This problem has 96 design variables ($N_f = 40$ relative to α , $N_e = 56$ relative to β).

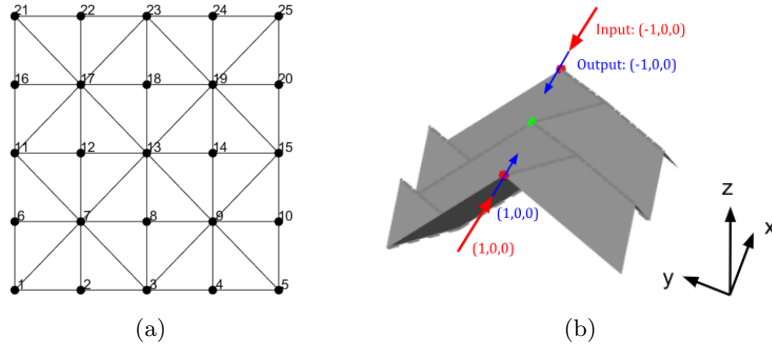


Fig. 6: Starting configuration of the Miura-Ori pattern. **(a)** Reference grid; **(b)** Load and boundary conditions ($L_x = 1.0\text{ m}$, $L_y = 1.0\text{ m}$, $F = 600\text{ N}$).

Tab. 2 displays that, when $m_0 = 0$ the axial rigidity remains constant and equal to EA_0 for all the trusses, therefore the second set of design variables is not considered. However, maintaining l_0 constant and equal to 0.50 and increasing m_0 (from 0.30 to 0.50), more trusses are allowed to have a minimum axial rigidity. As a result, the structure becomes more flexible and can sustain the targeted larger displacement, even for the cost of more iteration steps, as shown in Fig. 7. This indicates that the newly introduced optimization method leads to a more significant actuation with respect to the one in Reference [11].

Lastly, as mentioned in the previous example, even if the load condition and l_0 are kept constant during this analysis, due to the complexity of this configuration a more flexible structure implies that the origami needs to be folded along different fold lines, leading to new optimized crease patterns.

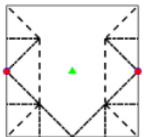
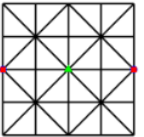
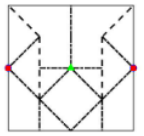
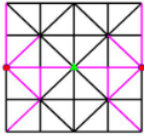
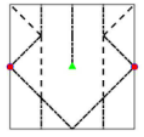
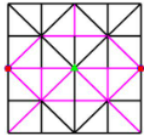
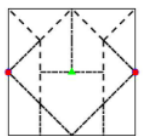
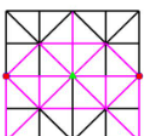
l_0 [-]	m_0 [-]	Optimized Crease Pattern	Axial Rigidity distribution	f [mm]
1 set of design variables (a)				
0.50	0			-38.00
2 sets of design variables (a, β)				
0.50	0.30			-76.80
0.50	0.40			-87.20
0.50	0.50			-94.00

Table 2: Final configurations of the Miura-Ori fold pattern. Dashed lines in Optimized Crease Pattern: active folds with $G = G_{soft} = 10^2 Pa \cdot m^2$. Magenta and black lines in Axial Rigidity Distribution: $EA = EA_{min} = 10^4 Pa \cdot m^2$ and $EA = EA_0 = 10^8 Pa \cdot m^2$.

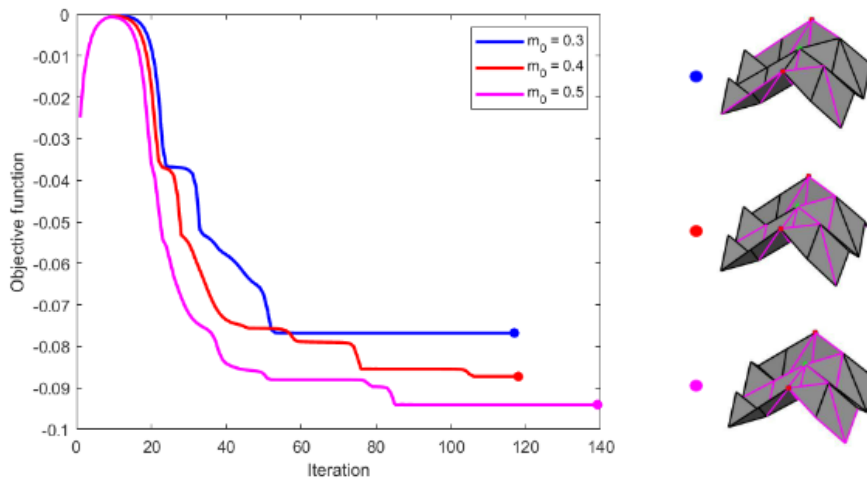


Fig. 7: Objective function over iteration for different m_0 ($l_0 = 0.5$).

3 Topology Optimization based on Nonlinear Analysis

In large displacement origami, the structure does not follow the traditional linear mechanics, and a different optimization method than the one described in the previous Section is needed.

Gillman et al. [15] successfully introduced a modified nonlinear truss model to consider large displacements and large rotations in origami, while optimizing efficiency and accuracy to face the increased difficulty given by the nonlinearity of the problem. This model is based on the positional finite element truss by Greco et al. [16], which presented a geometric nonlinear formulation for static problems involving space trusses, based on the finite element method (FEM), that uses nodal positions rather than nodal displacements to describe the problem. The model was modified including a torsional spring around the truss element, so that the fold stiffness between two adjacent facets can be considered.

Liu and Paulino [13] also introduces a torsional spring in their analysis, however using nodal displacements rather than nodal positions to describe the problem. Nevertheless, the positional formulation is simpler and more advantageous for the assignment of position-based constraints and a more direct representation of the fold angles.

A scheme of the origami element of the modified nonlinear truss model is shown in Fig. 8, where:

- The fold angle ϕ is the dihedral angle that defines the inclination of a facet with respect to its original position;
- $\mathbf{X}_l = (X_l, Y_l, Z_l)$ (with $l = 1, \dots, 4$) is the global position of the l -th node.
 $X_{tri} = \{\mathbf{X}_1, \mathbf{X}_2, \mathbf{X}_3, \mathbf{X}_4\}$ is the set of global coordinates of the local nodes required to define the fold angle ϕ ;
- The black line that connects nodes 1 and 2 is the fold line, a truss element that contains an axial strain term with axial rigidity EA and a bending energy term with fold stiffness G ;
- $\mathbf{F}_i = (F_{X_i}, F_{Y_i}, F_{Z_i})$ is the nodal force applied in one of the nodes of the fold line;
- ζ is the nondimensional integration length dimension along the axis of the truss.

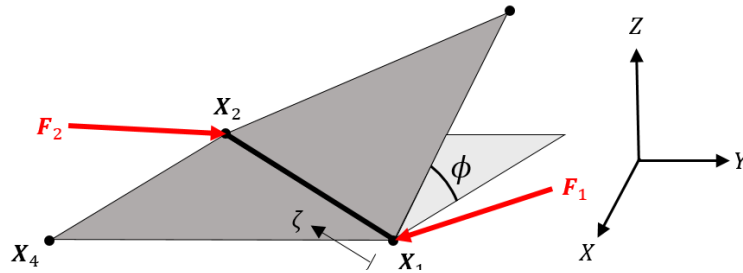


Fig. 8: Scheme of the origami element in the modified nonlinear truss model.

3.1 Principle of Minimum Energy

To study the nonlinear problem, the principle of minimum energy associated with the single element in Fig. 8 is presented, and it can be extended to a generic origami truss structure through assembly. The total energy (Π) is defined as

$$\Pi = U_t - P, \quad (18)$$

where U_t is the potential energy and P is the external energy.

The potential energy is

$$U_t = t_0 \int_0^1 \left[\frac{EA}{2} \varepsilon(\mathbf{X}_1, \mathbf{X}_2)^2 + \frac{G}{2} \tilde{\phi}(\mathbf{X}_1, \mathbf{X}_2, \mathbf{X}_3, \mathbf{X}_4)^2 \right] d\zeta = t_0 \int_0^1 [u_t + u_h] d\zeta. \quad (19)$$

The axial strain ε quantifies the axial deformation of the truss element

$$\varepsilon = \frac{1}{t_0} (|\mathbf{X}_2 - \mathbf{X}_1| - t_0) = \frac{1}{t_0} (\sqrt{(X_2 - X_1)^2 + (Y_2 - Y_1)^2 + (Z_2 - Z_1)^2} - t_0), \quad (20)$$

while $\tilde{\phi}$ quantifies the torsional deformation of the spring

$$\tilde{\phi}(\mathbf{X}_1, \mathbf{X}_2, \mathbf{X}_3, \mathbf{X}_4) = \phi(\mathbf{X}_1, \mathbf{X}_2, \mathbf{X}_3, \mathbf{X}_4) - \phi_0, \quad (21)$$

where t_0 and ϕ_0 are the length and the angle of the structure in their undeformed state, while ϕ is a nonlinear function that represents the current fold angle. A linear constitutive model is assumed in Eq.s (20) and (21), however ε and $\tilde{\phi}$ depend on the global position of the nodes, hence they are subjected to the geometric nonlinearities of the motion. Therefore, a penalty function is introduced to avoid singularities and to enforce that the two facets are kept in contact. Introducing the penalty function, the potential energy becomes

$$U_t^p = t_0 \int_0^1 [u_t + p(\phi)u_h] d\zeta, \quad (22)$$

hence, the total energy

$$\Pi = U_t^p - P. \quad (23)$$

The external energy is

$$P = F_{X_1}(X_1 - X_1^0) + F_{X_2}(X_2 - X_2^0) + F_{Y_1}(Y_1 - Y_1^0) + F_{Y_2}(Y_2 - Y_2^0) + F_{Z_1}(Z_1 - Z_1^0) + F_{Z_2}(Z_2 - Z_2^0), \quad (24)$$

where for example X_1^0 is the node location along the X axis of node 1 in the undeformed state. The forces are therefore multiplied by the displacements of the nodes: $\mathbf{u}_1 = \mathbf{X}_1 - \mathbf{X}_1^0$ and $\mathbf{u}_2 = \mathbf{X}_2 - \mathbf{X}_2^0$.

Lastly, the principle of minimum energy states that the equilibrium state of the structure is reached when the following equation is satisfied

$$\frac{\partial \Pi}{\partial X_l} = t_0 \int_0^1 \left[\frac{EA}{2} \frac{d\varepsilon}{dX_l} + \left(Gp(\phi)\tilde{\phi} + G\frac{\tilde{\phi}^2}{2} \frac{\partial p(\phi)}{\partial \phi} \right) \frac{\partial \phi}{\partial X_l} \right] d\zeta - F_{X_l} = q_l - F_{X_l} \quad (25)$$

$$= 0.$$

3.2 Linearization of the nonlinear problem

The principle of minimum energy introduces a system of nonlinear equations. To numerically solve them, the Newton-Raphson method is applied. Linearizing Eq. (25) through a Taylor's series expansion the residual $R_l(X_{tri})$ is obtained

$$R_l(X_{tri}) = \frac{\partial \Pi}{\partial X_l} = q_l(X_{tri}) - F_l = 0; \quad (26)$$

$$R_l(X_{tri}) \approx R_l(X_{tri}^0) + \nabla R_l(X_{tri}^0) \Delta X_{tri} = 0,$$

where the term $\nabla R_l(X_{tri}^0)$ is the tangent stiffness

$$K_{lm} = \nabla R_l(X_{tri}^0) = t_0 \int_0^1 \left[\frac{EA}{2} \frac{d^2\varepsilon}{dX_l dX_m} + Gp(\phi) \left(\frac{\partial \phi}{\partial X_m} \frac{\partial \phi}{\partial X_l} + \tilde{\phi} \frac{\partial^2 \phi}{\partial X_m \partial X_l} \right) \right. \quad (27)$$

$$\left. + G\frac{\partial^2 p(\phi)}{\partial \phi^2} \frac{\tilde{\phi}^2}{2} \left(\frac{\partial \phi}{\partial X_m} \frac{\partial \phi}{\partial X_l} + \tilde{\phi} \frac{\partial^2 \phi}{\partial X_m \partial X_l} \right) + 2G\tilde{\phi} \frac{\partial p(\phi)}{\partial \phi} \left(\frac{\partial \phi}{\partial X_m} \frac{\partial \phi}{\partial X_l} \right) \right] d\zeta.$$

where the indices l and m iterate through all the components of \mathbf{X}_{tri} . Therefore, from Eq. (26), the following equation is obtained

$$K_{lm} \Delta X_{tri} = -R_l(X_{tri}^0), \quad (28)$$

that is solved iteratively until the equilibrium is reached (within a set tolerance).

Furthermore, at each iteration, the residual R_l and the tangent stiffness K_{lm} are computed both for the trusses at the interior (fold lines) and for the trusses at the boundary, since those at the boundary do not fold, hence their bending energy term (the fold stiffness G) is equal to zero. They are later summed like in Eq.s (29) and (30) to obtain the global residual and the global tangent stiffness

$$R_l = R_l^F + R_l^B; \quad (29)$$

$$K_{lm} = K_{lm}^F + K_{lm}^B. \quad (30)$$

Lastly, increment loads are considered in this Chapter in order to follow the complex nonlinear loading behavior of origami structures subjected to large displacements. During every iterative cycle, the load is increased until a set number of iterations is

reached, taking into account that the maximum load magnitude applied should be of the same order as the fold stiffness, in order to allow the structure to be folded while suppressing too large deformations of truss members, leading to more realistic designs.

However, to explore more complex behaviors of origami structures with intricate nonlinear profiles, using a monotonically increasing force field is not enough. In these cases, an arc-length method, first introduced by Riks [17, 18] and Wempner [19] and later employed by Gillman et al. [15], should be applied, where a scalar Lagrange multiplier is introduced to scale the applied force vector.

3.3 Optimization Framework

Similarly to what Fuchi et al. [11] did with linear analysis, Gillman et al. [25] proposed a design method to apply nonlinear analysis to origami structures using topology optimization considering the fold stiffness of every truss element in the structure (modeled through the torsional spring stiffness G) as a design variable. Through this method, the optimized crease pattern is obtained, revealing only the active fold lines required to obtain the greatest actuation after the analysis. Furthermore, even if the inactive fold lines are not shown, they indicate that the two adjacent facets are considered as one, therefore, if their angle ϕ is not zero, it is possible to observe a coarse representation of *facet bending*. The fold stiffness is displayed in Eq. (6).

Following the linear method described in the previous Section, here the optimization method introduced by Gillman et al. [25] is improved including also the axial rigidity EA as a design variable through the SIMP method, considering Eq. (8).

Nevertheless, due to the nonlinearity of the problems, this method does not provide only black-and-white results, leading also to some in-between values.

The *optimization problem* is the following:

<p>Find $\mathbf{x} = \alpha_1, \dots, \alpha_{N_f}, \beta_1, \dots, \beta_{N_e}$ that</p> <p>Minimize $f = -\mathbf{c}^T \mathbf{u}$</p> <p>Subject to</p> $g_1 = v_{0,1} - \frac{1}{N_f} \sum_{i=1}^{N_f} x_i \leq 0; \quad g_2 = v_{0,2} - \frac{1}{N_e} \sum_{i=N_f+1}^{N_f+N_e} x_i \leq 0; \quad (31)$ $0 \leq x_i \leq 1; \quad \forall i = 1, \dots, N_f + N_e;$ $R_l(\mathbf{X}) = 0; \quad u_l = X_l - X_l^0; \quad l = 1, \dots, 3N_n.$
--

The difference with the linear optimization in the previous Section lies in the governing equation of the system. The final constraint is the linearization of the residual to solve the system of nonlinear equations introduced in Eq. (25), where the distance between the deformed and undeformed location of the l -th node is the displacement of that node. Lastly, N_n is the number of nodes, hence $3N_n$ are the degrees of freedom of the structure.

Two gradient-based optimization algorithms are used in the analyses: the Method of Moving Asymptotes (MMA) and the Sequential Quadratic Programming (SQP). An overview of the algorithm is shown in Fig. 9.

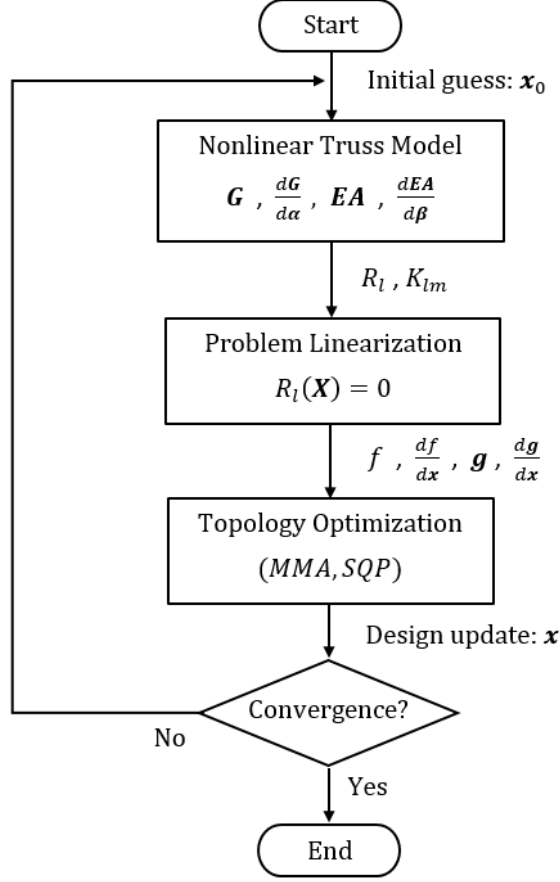


Fig. 9: Flow chart of the linear optimization process.

3.3.1 Sensitivity analysis

To carry out the sensitivity analysis, the derivative of the objective function with respect to the design variables is obtained as follows:

$$\frac{df}{dx_i} = \frac{\partial f}{\partial x_i} + \frac{\partial f}{\partial X_m} \frac{dX_m}{dx_i}, \quad (32)$$

where $\partial f/\partial x_i = 0$ since f does not explicitly depend on x_i , $\partial f/\partial X_m$ is found by directly differentiating the objective function f and dX_m/dx_i is determined solving

the following system of equations:

$$K_{lm} \frac{dX_m}{dx_i} = -\frac{\partial R_l}{\partial x_i}. \quad (33)$$

The vector $\partial R_l / \partial x_i \in [3N_n, N_f + N_e]$ has the first N_f columns equal to

$$\frac{\partial R_l}{\partial \alpha_k} = t_0 \int_0^1 \left[\frac{\partial G_k}{\partial \alpha_k} p(\phi) \tilde{\phi} + \frac{\partial G_k}{\partial \alpha_k} \frac{\tilde{\phi}^2}{2} \frac{\partial p(\phi)}{\partial \phi} \right] \frac{\partial \phi}{\partial X_l} d\zeta, \quad (34)$$

where

$$\frac{\partial G_k}{\partial \alpha_k} = (a_1 - a_0) 10^{a_0 + \alpha_k (a_1 - a_0)} \log(10), \quad (35)$$

while the remaining N_e columns are equal to

$$\frac{\partial R_l}{\partial \beta_j} = t_0 \int_0^1 \frac{1}{2} \frac{\partial EA_j}{\partial \beta_j} \frac{d\varepsilon}{dX_l} d\zeta, \quad (36)$$

where

$$\frac{\partial EA_j}{\partial \beta_j} = p \beta_j^{(p-1)} (EA_0 - EA_{min}). \quad (37)$$

The whole process, schematized in Fig. 9, is described here:

1. At the start of each iteration, \mathbf{G} , \mathbf{EA} and their gradients are computed for each fold line and truss member respectively. The residual R_l and the tangent stiffness K_{lm} are evaluated from Eq.s (26) and (27), along with the gradient of the residual $\partial R_l / \partial x_i$ from Eq.s (34) and (36);
2. Through Eq. (30), the nonlinear problem is linearized with the purpose of finding the displacement field ΔX_{tri} , while its gradient is obtained from Eq. (33);
3. The objective function and its gradient from Eq.s (31) and (32) are computed, as well as the constraint functions and their gradients from Eq.s (10) and (11);
4. The gradient-based topology optimization is carried out both with the MMA and the SQP method, in order to obtain the new set of design variables \mathbf{x} for the next iteration;
5. This iterative process is repeated until the equilibrium state of the structure is reached, i.e. the relative error between the objective functions at the current and at the previous iteration is lower than a set tolerance.

3.4 Numerical Examples

To assess the capability of the nonlinear truss model with the introduction of axial rigidity as a design variable, two different starting configurations of well-known origami actuator designs (“Chomper” and “Square Twist” patterns) are studied. The optimization is evaluated through comparisons with the works of Gillman et al. [24, 25], where only one set of design variables is considered. Each case is studied first using the Origami Topology Optimization with Nonlinear Truss Model (OTON) in Reference [36] that uses only the fold stiffness exponent (α) as design variable and the constraint

on the number of active fold lines allowed (l_0), then with a modified OTON, which uses the method described in this Section, that also considers the axial rigidity density (β) as design variable and the constraint on the number of trusses that are allowed to have a minimum axial rigidity (m_0).

Furthermore, the dashed lines in the optimized crease pattern indicate the active folds that remain after the optimization (soft folds with $G = G_{soft}$). Lastly, the color of the trusses in the axial rigidity distribution is given in a scale of gray, where white and black indicate an axial rigidity $EA = EA_{min}$ or $EA = EA_0$ respectively. However, a "projected" axial rigidity distribution is presented, where the black and magenta lines indicate that the truss members have an axial rigidity with a relative error within 10% close to $EA = EA_0$ or $EA = EA_{min}$ respectively, while greater than 10% for the gray lines.

3.4.1 Chomper fold pattern

The first example considers a simple *Chomper*, a famous fold pattern that has been used as a gripping mechanism [37]. The problem has 48 design variables ($N_f = 18$ relative to α , $N_e = 30$ relative to β). Fig. 10a shows the reference grid of the structure, while Fig. 10b shows the three-dimensional representation of the starting configuration with the load and boundary conditions, where the central green triangle is a fixed node, while the other two are allowed to move along x .

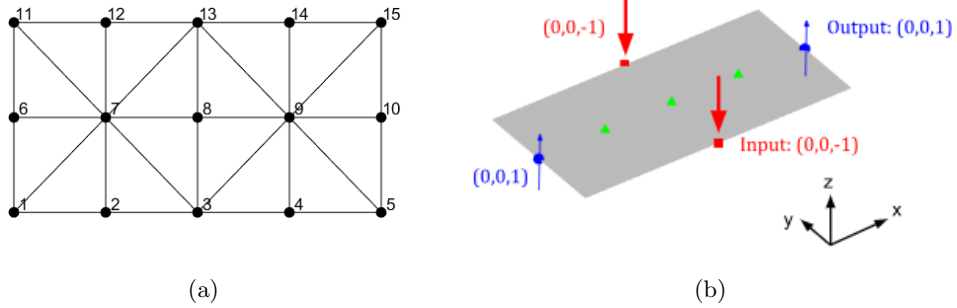


Fig. 10: Starting configuration of the Chomper pattern. (a) Reference grid; (b) Load and boundary conditions ($L_x = 0.2 \text{ m}$, $L_y = 0.2 \text{ m}$, $F = 10\,000 \text{ N}$).

In this example, the following parameters are considered:

- $EA = 10^7 \text{ Pa} \cdot \text{m}^2$ for one set of design variables;
- $EA_{min} = 10^5 \text{ Pa} \cdot \text{m}^2$ and $EA_0 = 10^7 \text{ Pa} \cdot \text{m}^2$ for two sets of design variables;
- $l_0 = 0.44$ (equivalent to 6 active fold lines allowed);
- $G_{stiff}/G_{soft} = 10^3$.

To demonstrate the effect that material properties have on the optimal actuation motion, two sets of material properties are considered, varying G_{soft} and G_{stiff} :

1. Case 1: $EA/G_{stiff} = 10^1$ (or $EA_0/G_{stiff} = 10^1$ for two sets of design variables);
2. Case 2: $EA/G_{stiff} = 10^3$ (or $EA_0/G_{stiff} = 10^3$ for two sets of design variables).

For each case, different values of the constraint m_0 are used to study the effect of the addition of the second set of design variables.

Case 1

Tab. 3 shows the values of the objective functions and the final configurations of the Chomper problem for Case 1 obtained with the MMA method.


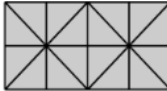
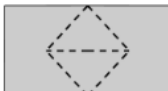
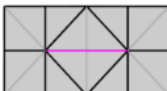
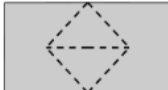
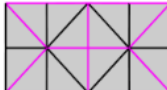
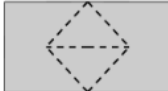
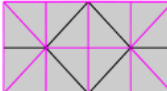
l_0 [-]	m_0 [-]	Optimized Crease Pattern	Projected Axial Rigidity distribution	f [mm]
1 set of design variables (a)				
0.44	0			- 52.92
2 sets of design variables (a, β)				
0.44	0.20			- 88.30
0.44	0.50			- 92.84
0.44	0.80			- 92.92

Table 3: Final configurations of the Chomper pattern - Case 1. Dashed lines in Optimized Crease Pattern: active folds with $G = G_{soft} = 10^3 Pa \cdot m^2$. Magenta and black lines in Projected Axial Rigidity Distribution: $EA = EA_{min} = 10^5 Pa \cdot m^2$ and $EA = EA_0 = 10^7 Pa \cdot m^2$.

All the configurations in Tab. 3 discover the Chomper fold pattern. Like in the linear case, if m_0 is increased more trusses are allowed to have a minimum axial rigidity, thus leading to a more flexible structure that can sustain larger displacements but with more iteration steps, as shown in Fig. 11.

The improvement of the described nonlinear method with respect to the linear method in the previous Section is evident, since greater displacements than within a 10% range of the length of the structure can now be obtained. Therefore, even

though the load and boundary conditions in Fig. 10b penalize the stretching of the trusses in the small displacement analysis (emphasizing only the effect of the folding of the sheet), for the large displacements in the nonlinear analysis stretching becomes relevant and the effect of increasing m_0 can now be assessed.

The small ratio considered in Case 1 between the axial rigidity of the truss element and a stiff fold ($EA/G_{stiff} = 10^1$) favors facet stretching over facet bending since a greater fold stiffness G penalizes the bending of the structure. Therefore, continuous regions of the structure with G_{stiff} (area in sheet with no dashed lines) do not exhibit bending, and the structure appears to be slightly stretched along some trusses while compressed along others.

It must be noted that, for $l_0 = 0.44$, with one set of design variables (hence with the formulation in Reference [25]) the value of the objective function is $f = -52.92 \text{ mm}$, while with two sets of design variables is $f = -92.92 \text{ mm}$ (for $m_0 = 0.80$), thus with the topology optimization carried out with the method in this Section a greater actuation than the one in Reference [25] is obtained.

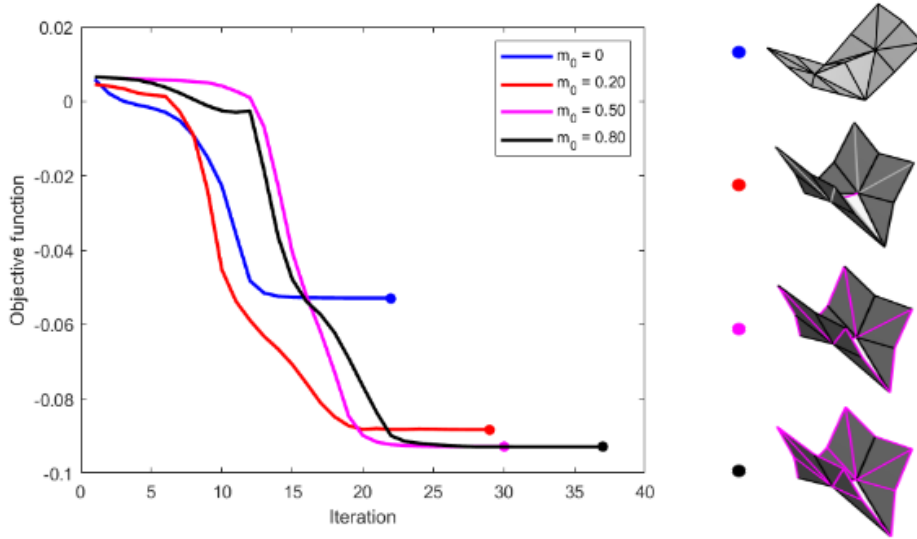


Fig. 11: Case 1, objective function over iteration for different m_0 ($l_0 = 0.44$).

It is also interesting to notice that, since the load condition and l_0 are kept constant during this analysis, the optimized crease pattern is the same for the considered material fractions.

Lastly, soft fold lines are not discovered between the fixed nodes since the facets that connect the input nodes to the fixed nodes form two symmetric moment arms that lead to the same motion, regardless of the fold stiffnesses of these elements. However, due to the large angle between these two faces, the soft fold lines are added in post-optimization.

Case 2

Tab. 4 shows the values of the objective functions and the final configurations of the Chomper problem for Case 2 obtained with the MMA method.


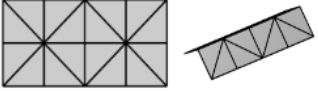

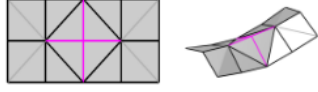

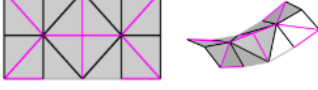
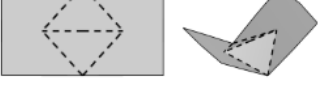

l_o [-]	m_o [-]	Optimized Crease Pattern	Projected Axial Rigidity distribution	f [mm]
1 set of design variables (a)				
0.44	0			-9.0e-5
2 sets of design variables (a, β)				
0.44	0.20			-14.23
0.44	0.50			-18.79
0.44	0.80			-54.42

Table 4: Final configuration of the Chomper pattern - Case 2. Dashed lines in Optimized Crease Pattern: active folds with $G = G_{soft} = 10^1 Pa \cdot m^2$. Magenta and black lines in Projected Axial Rigidity Distribution: $EA = EA_{min} = 10^5 Pa \cdot m^2$ and $EA = EA_0 = 10^7 Pa \cdot m^2$.

The ratio considered in Case 2 between the axial rigidity of the trusses and a stiff fold ($EA/G_{stiff} = 10^3$) is larger than the one considered in Case 1, hence facet bending is favored over facet stretching. However, the gradient-based optimization using one set of design variables fails to discover an origami configuration that leads to positive vertical actuation in the output nodes. Fig. 12 shows that in this case the problem does not converge and the iterative process is stopped at 100 iterations, resulting in an objective function value close to zero.

Nevertheless, as shown in Tab. 4, using two sets of design variables it is possible to observe a vertical actuation of the output nodes and the bending of the structure (change in angle between some facets with no soft fold lines between them).

Furthermore, if m_o is increased, more trusses are allowed to have a minimum axial rigidity, thus the final configuration tends to lean toward that of Case 1. Therefore, for

$m_0 = 0.80$, the Chomper fold pattern is discovered, obtaining a larger actuation than with lower m_0 values, but for the cost of more iteration steps, as shown in Fig. 12.

Lastly, since the ratio EA/G_{stiff} decreases if m_0 increases, facet stretching tends to be more favored than facet bending. Therefore, for $m_0 = 0.80$ no bending can be observed in the structure.

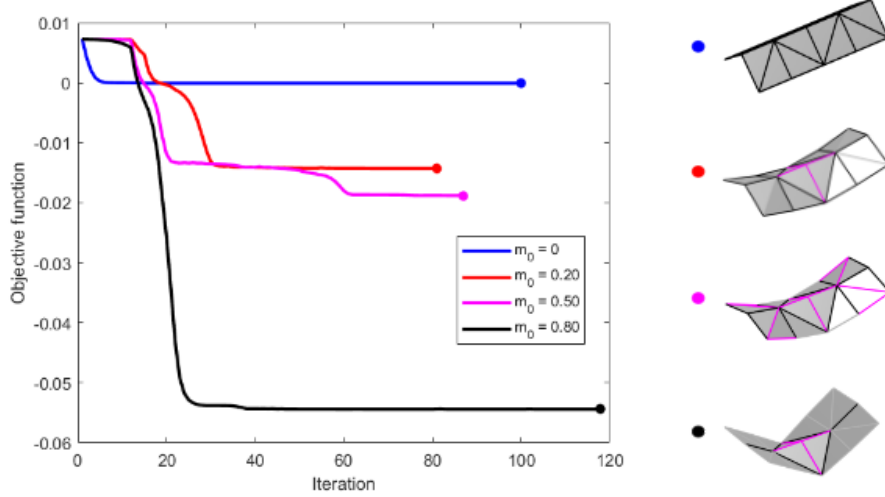


Fig. 12: Case 2, objective function over iteration for different m_0 ($l_0 = 0.44$).

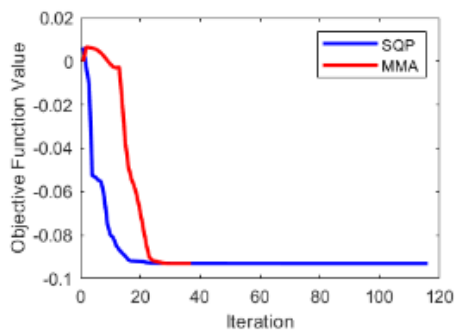
As mentioned in this Section, the SIMP method does not lead to a black-and-white solution for the problem, hence the axial rigidity EA of the trusses takes on values different from EA_{min} and EA_0 . Therefore, Tab. 5 shows the real axial rigidity distribution of the structure, where the color of the trusses in the axial rigidity distribution is given in a scale of gray, with white and black indicating an axial rigidity $EA = EA_{min}$ or $EA = EA_0$ respectively. Moreover, as expected, it can be observed that the color of the trusses becomes slightly lighter if m_0 is increased.

Lastly, the analysis is repeated with the SQP method, obtaining the same final configurations. In Fig. 13, both optimization methods converge to the same results, but the SQP method needs more iterations to converge due to its higher computational cost, as described by Fanni et al. [38].

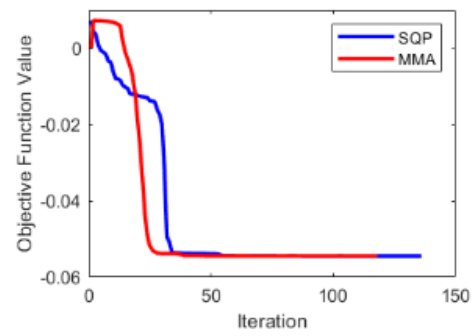
In order to discover the Chomper fold pattern, Gillman et al. [25] implements a Genetic Algorithm (GA) that enables the exploration of the bending phenomenon and obtains vertical actuation with less facet deformation. Although the superior performance of GA for these origami topology optimization problems, the trade-off is in the amount of computational cost required with respect to gradient-based methods, since four orders of magnitude more evaluations of the objective function are required.

l_0 [-]	m_0 [-]	Axial rigidity distribution		Colorbar
		Case 1	Case 2	
0.44	0.20			 EA_0 EA_{min}
0.44	0.50			
0.44	0.80			

Table 5: Axial rigidity distribution of Case 1 and Case 2 of the Chomper pattern.



(a)



(b)

Fig. 13: Objective function over iteration with SQP and MMA methods of the Chomper pattern, for $l_0 = 0.44$, $m_0 = 0.80$. (a) Case 1; (b) Case 2.

3.4.2 Square Twist fold pattern

The second example considers the famous *Square Twist* fold pattern, used for space antennas [39]. The problem has 96 design variables ($N_f = 40$ relative to α , $N_e = 56$ relative to β). The Square Twist pattern is shown in Fig. 14 for a geometry with a total of 176 fold lines.

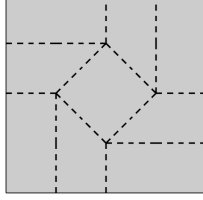


Fig. 14: Square Twist pattern for a geometry with 176 fold lines.

To minimize the computational cost, the geometry with a total of 40 fold lines depicted in the right part of Fig. 15 was chosen as the targeted Square Twist configuration.

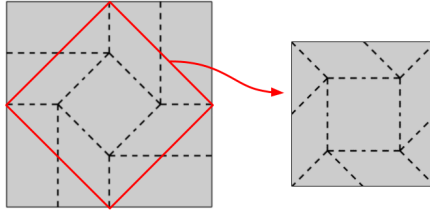


Fig. 15: Targeted Square Twist pattern (right) for a geometry with 40 fold lines.

Fig. 16a shows the reference grid of the structure, while Fig. 16b shows the three-dimensional representation of the starting configuration with the load and boundary conditions.

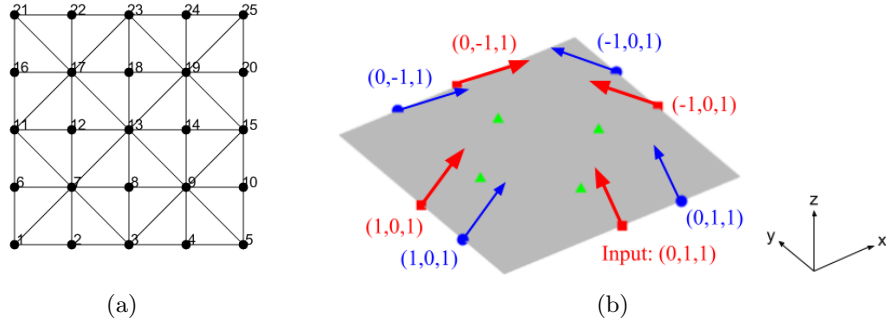


Fig. 16: Starting configuration of the Square Twist pattern. (a) Reference grid; (b) Load and boundary conditions ($L_x = 0.2 m$, $L_y = 0.2 m$, $F = 1000 N$).

The loads and boundary conditions in Fig. 16b should result in an inward folding followed by a twisting motion to achieve a flat folded configuration where the facets are parallel and in contact with each other.

In this example, the following parameters are considered:

- $EA_{min} = 10^6 Pa \cdot m^2$ and $EA_0 = 10^8 Pa \cdot m^2$;
- $l_0 = 0.40$ (equivalent to 16 active fold lines allowed);
- $m_0 = 0.43$ (equivalent to 24 trusses that are allowed to have axial rigidity $EA = EA_{min}$);
- $EA_0/G_{stiff} = 10^4$;
- $G_{stiff}/G_{soft} = 10^3$.

Again, the optimization was carried out both with MMA and SQP methods. However, using the conventional method with only one set of design variables, it is not possible to reach convergence, hence the targeted origami configuration cannot be found. The reason for this is that one of the key aspects of the Square Twist pattern is that it cannot be folded rigidly, thus, if the trusses are made too stiff, it would not be able to fold [40].

The addition of axial rigidity as a design variable with the proposed method allows to obtain a more elastic folding motion of the origami sheet, therefore the present case study can be analyzed. Nevertheless, the objective function obtained with MMA oscillates reaching uncertain results since it presents multiple subsequent local minima between the lower and upper bounds of the approximated objective function at each iteration. Therefore, only the final configuration obtained with the SQP method is presented in Fig. 17.

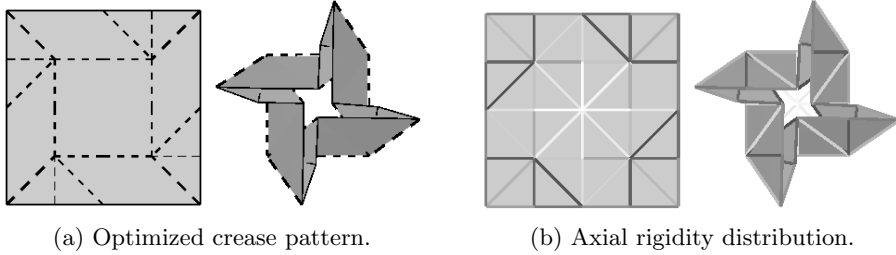


Fig. 17: Final configuration of the Square Twist pattern. Dashed lines in Optimized Crease Pattern: active folds with $G = G_{soft} = 10^1 Pa \cdot m^2$. White and black lines in Axial Rigidity Distribution: $EA = EA_{min} = 10^6 Pa \cdot m^2$ and $EA = EA_0 = 10^8 Pa \cdot m^2$. Value of the objective function: $f = -0.4829 mm$.

As it can be noted, the optimized crease patterns in Fig. 17a fail to satisfy the constraint on the allowable number of active fold lines (l_0), since the number of active fold lines obtained after the optimization process is greater than 40%. This is likely due to numerical instability phenomena during the optimization process related to the nonlinearity of the problem. Therefore, the results need to be projected. The 16 fold

lines (corresponding to $l_0 = 0.40$) with the lowest fold stiffnesses and the 24 trusses (corresponding to $m_0 = 0.43$) with the lowest axial rigidities are selected. The values of α relative to these folds and that of β relative to these trusses are set equal to 0, while the remaining values are set to 1. The results obtained after the projection are displayed in Fig. 18.

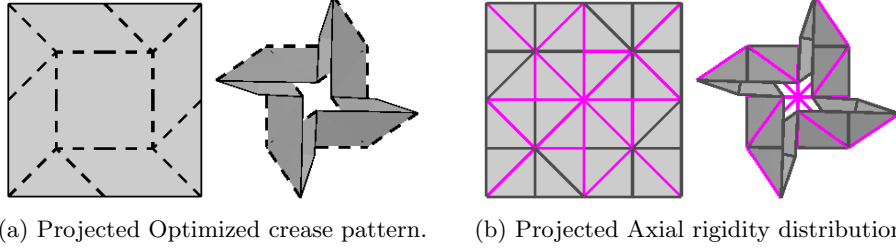


Fig. 18: Projected final configuration of the Square Twist pattern. Dashed lines in Optimized Crease Pattern: active folds with $G = G_{soft} = 10^1 Pa \cdot m^2$. Magenta and black lines in Projected Axial Rigidity Distribution: $EA = EA_{min} = 10^6 Pa \cdot m^2$ and $EA = EA_0 = 10^8 Pa \cdot m^2$.

This result shows that, using the proposed improved method for the present case study, it is possible to obtain the targeted Square Twist configuration, with a distribution of axial rigidity among the trusses as shown in Fig. 18b. This origami pattern could only be obtained, in conventional methods, using non-gradient-based topology optimizations, like the Genetic Algorithm (GA). Therefore, the proposed method allows to obtain promising origami designs using gradient-based topology optimization, significantly decreasing the computational cost.

4 Conclusion

The presented work aimed to improve a design methodology to enhance the performance of origami structures using topology optimization, including axial rigidity as a design variable. A truss model was used as test case where origami are constituted by truss elements connected by pin joints.

First, a linear analysis is carried out, providing a low computational cost model effective in analyzing origami structures at the initiation of folding. Subsequently, a nonlinear analysis model is utilized to consider large displacements and large rotations while optimizing the efficiency and accuracy of the results.

Previous works on topology optimization of origami structures have only considered fold stiffness relative to the bending energy as a design variable, focusing on minimizing the number of fold lines that must remain active during the folding motion while maximizing the actuation of the structure at selected nodes. The novelty of this work is in the introduction of axial rigidity of the trusses as a second design variable. Although this leads to a slight increase in the design complexity, the optimization process is now improved since new configurations can be analyzed.

The capabilities of the model were assessed through study cases of well-known origami fold patterns, comparing the results obtained from previous works that considered only fold stiffness as design variable, to the ones obtained using also axial rigidity as design variable with the introduced improved method.

The study demonstrates that, if the axial rigidity is allowed to vary among the trusses of the structure, it is possible to expand the design space and explore new configurations for origami structures, since each truss is allowed to stretch and compress in an optimized way. Also, if the number of fold lines with minimum axial rigidity is increased, the structure becomes more flexible and can sustain a targeted larger actuation. Lastly, with a variable axial rigidity, multi-material topology optimization can be achieved and new promising designs for origami structures can be discovered.

4.1 Future Work

The presented study can be expanded to maximize its effectiveness and application.

Origami structures usually present repeating patterns. These configurations could be examined considering periodic boundary conditions in the design process.

To explore more complex behaviors of origami structures with intricate nonlinear profiles and to capture origami equilibrium paths beyond limit points, an arc-length method with a scalar Lagrange multiplier needs to be applied to the optimization process.

Origami usually exhibit equilibrium bifurcations off the flat state. Hence, to explore these phenomena, the described method can be improved including modal analysis.

Lastly, using topology optimization for analyzing origami structures can be functional to the discovery of auxetic metamaterials. Therefore the presented method could lead to the design of new origami patterns that manifest a negative Poisson's ratio.

Acknowledgments. We are grateful to Dr. Kazuko Fuchi from the University of Dayton for her advice and for providing the MATLAB codes in [35] and [36]. The authors acknowledge Fundação para a Ciência e a Tecnologia (FCT), through IDMEC, 504 under LAETA, project UIDB/50022/2020. Also, A.S. acknowledges the funding provided by the NSERC Canada Research Chair program.

Declarations

Funding. Natural Sciences and Engineering Research Council of Canada, 950 - 233175.

Conflict of interest. The authors declare that they have no conflicts of interest.

Ethics approval. When carrying out the study, we followed all applicable ethical requirements.

Consent to participate. All authors have approved this study's publication.

Consent for publication. We agree with all publication policies of the journal.

Data availability. The MATLAB codes used during the current study will be made available from the authors upon request.

Authors' contributions. This work is based on the master thesis of V. Cretella, who modified the MATLAB code in Ref. [35] and [36] to obtain the results. A. Suleman, A. Sohoulı and A. Pagani were the supervisors, who guided the student throughout the study.

Replication of results. The main results of this study can be reproduced by using the MATLAB codes used in this paper, available upon request. The values of the parameters used can be found in this paper.

References

- [1] Miura, K., Natori, M.: 2-d array experiment on board a space flyer unit. *Space Solar Power Review* **5**(4), 345–356 (1985)
- [2] Lang, R.J.: Origami: Complexity in creases (again). *Engineering and Science* **67**(1), 5–19 (2004)
- [3] Häuplik, S., Gruber, P., Imhof, B., Özdemir, K., Waclavicek, R., Perino, M.A.: Deployable structures for a human lunar base. In: 57th International Astronautical Congress, pp. 3–2
- [4] Lebéé, A.: From folds to structures, a review. *International journal of space structures* **30**(2), 55–74 (2015)
- [5] Hull, T.C., *et al.*: Modelling the folding of paper into three dimensions using affine transformations. *Linear Algebra and its applications* **348**(1-3), 273–282 (2002)
- [6] Peraza Hernandez, E.A., Hartl, D.J., Lagoudas, D.C.: *Active origami: modeling, design, and applications*. Cham: Springer (2018)
- [7] Tachi, T.: Simulation of rigid origami. *Origami* **4**(08), 175–187 (2009)
- [8] Peraza Hernandez, E.A., Hartl, D.J., Lagoudas, D.C.: Kinematics of origami structures with smooth folds. *Journal of Mechanisms and Robotics* **8**(6), 061019 (2016)
- [9] Schenk, M., Guest, S.D., *et al.*: Origami folding: A structural engineering approach. *Origami* **5**, 291–304 (2011)
- [10] Fuchi, K., Buskohl, P.R., Joo, J.J., Reich, G.W., Vaia, R.A.: Topology optimization for design of origami-based active mechanisms. In: *International Design Engineering Technical Conferences and Computers and Information in Engineering Conference*, vol. 46377, pp. 05–08049 (2014). American Society of Mechanical Engineers
- [11] Fuchi, K., Buskohl, P.R., Bazzan, G., Durstock, M.F., Reich, G.W., Vaia, R.A., Joo, J.J.: Origami actuator design and networking through crease topology optimization. *Journal of Mechanical Design* **137**(9), 091401 (2015)

- [12] Filipov, E., Liu, K., Tachi, T., Schenk, M., Paulino, G.H.: Bar and hinge models for scalable analysis of origami. *International Journal of Solids and Structures* **124**, 26–45 (2017)
- [13] Liu, K., Paulino, G.H.: Nonlinear mechanics of non-rigid origami: an efficient computational approach. *Proceedings of the Royal Society A: Mathematical, Physical and Engineering Sciences* **473**(2206), 20170348 (2017)
- [14] Filipov, E.T., Paulino, G.H., Tachi, T.: Origami tubes with reconfigurable polygonal cross-sections. *Proceedings of the Royal Society A: Mathematical, Physical and Engineering Sciences* **472**(2185), 20150607 (2016)
- [15] Gillman, A., Fuchi, K., Buskohl, P.: Truss-based nonlinear mechanical analysis for origami structures exhibiting bifurcation and limit point instabilities. *International Journal of Solids and Structures* **147**, 80–93 (2018)
- [16] Greco, M., Gesualdo, F.A.R., Venturini, W.S., Coda, H.B.: Nonlinear positional formulation for space truss analysis. *Finite elements in analysis and design* **42**(12), 1079–1086 (2006)
- [17] Riks, E.: The application of newton’s method to the problem of elastic stability (1972)
- [18] Riks, E.: An incremental approach to the solution of snapping and buckling problems. *International journal of solids and structures* **15**(7), 529–551 (1979)
- [19] Wempner, G.A.: Discrete approximations related to nonlinear theories of solids. *International Journal of Solids and Structures* **7**(11), 1581–1599 (1971)
- [20] Leon, S.E., Paulino, G.H., Pereira, A., Menezes, I.F., Lages, E.N.: A unified library of nonlinear solution schemes (2011)
- [21] Leon, S.E., Lages, E.N., De Araújo, C.N., Paulino, G.H.: On the effect of constraint parameters on the generalized displacement control method. *Mechanics Research Communications* **56**, 123–129 (2014)
- [22] Tachi, T., Hull, T.C.: Self-foldability of rigid origami. *Journal of Mechanisms and Robotics* **9**(2), 021008 (2017)
- [23] Santangelo, C.D.: Extreme mechanics: Self-folding origami. *Annual Review of Condensed Matter Physics* **8**, 165–183 (2017)
- [24] Gillman, A., Fuchi, K., Bazzan, G., Alyanak, E.J., Buskohl, P.R.: Discovering origami fold patterns with optimal actuation through nonlinear mechanics analysis. In: *International Design Engineering Technical Conferences and Computers and Information in Engineering Conference*, vol. 58189, pp. 05–08052 (2017). American Society of Mechanical Engineers

- [25] Gillman, A.S., Fuchi, K., Buskohl, P.R.: Discovering sequenced origami folding through nonlinear mechanics and topology optimization. *Journal of Mechanical Design* **141**(4), 041401 (2019)
- [26] Gillman, A., Fuchi, K., Cook, A., Pankonien, A., Buskohl, P.R.: Topology optimization for discovery of auxetic origami structures. In: *International Design Engineering Technical Conferences and Computers and Information in Engineering Conference*, vol. 51814, pp. 05–07059 (2018). American Society of Mechanical Engineers
- [27] Yue, S.: A review of origami-based deployable structures in aerospace engineering. In: *Journal of Physics: Conference Series*, vol. 2459, p. 012137 (2023). IOP Publishing
- [28] Svanberg, K.: The method of moving asymptotes—a new method for structural optimization. *International journal for numerical methods in engineering* **24**(2), 359–373 (1987)
- [29] Gill, P.E., Murray, W., Wright, M.H.: *Numerical Linear Algebra and Optimization*. SIAM, ??? (2021)
- [30] Andreassen, E., Clausen, A., Schevenels, M., Lazarov, B.S., Sigmund, O.: Efficient topology optimization in matlab using 88 lines of code. *Structural and Multidisciplinary Optimization* **43**, 1–16 (2011)
- [31] Schenk, M., Guest, S.D.: Origami folding: A structural engineering approach. In: *5OSME, 5th International Conference on Origami in Science, Mathematics and Education*. Retrieved From: [Http://www. Markschenk. Com/research/# Papers](http://www.Markschenk.Com/research/#Papers) (2010)
- [32] Nazir, A., Gokcekaya, O., Billah, K.M.M., Ertugrul, O., Jiang, J., Sun, J., Husain, S.: Multi-material additive manufacturing: A systematic review of design, properties, applications, challenges, and 3d printing of materials and cellular metamaterials. *Materials & Design*, 111661 (2023)
- [33] Suzuki, K., Kikuchi, N.: A homogenization method for shape and topology optimization. *Computer methods in applied mechanics and engineering* **93**(3), 291–318 (1991)
- [34] Rozvany, G.I., Zhou, M., Birker, T.: Generalized shape optimization without homogenization. *Structural optimization* **4**, 250–252 (1992)
- [35] Fuchi, K.: Origami Mechanism Topology Optimizer (OMTO) Ver 1.1n. MATLAB Central File Exchange, Accessed on May 8, 2023 (2015). <https://www.mathworks.com/matlabcentral/fileexchange/53037-origami-mechanism-topology-optimizer-omto-ver-1-1n>

- [36] Gillman, A., Fuchi, K., Buskohl, P.: Origami Topology Optimization w/ Nonlinear Truss Model. MATLAB Central File Exchange, Retrieved December 5, 2018, Accessed on July 6, 2023 (2018). <https://www.mathworks.com/matlabcentral/fileexchange/69612-origami-topology-optimization-w-nonlinear-truss-model>
- [37] Edmondson, B.J., Bowen, L.A., Grames, C.L., Magleby, S.P., Howell, L.L., Bateman, T.C.: Oriceps: Origami-inspired forceps. In: Smart Materials, Adaptive Structures and Intelligent Systems, vol. 56031, pp. 001–01027 (2013). American Society of Mechanical Engineers
- [38] Fanni, M., Shabara, M., Alkalla, M.: A comparison between different topology optimization methods. MEJ. Mansoura Engineering Journal **38**(4), 13–24 (2020)
- [39] Rubio, A.J., Kaddour, A.-S., Georgakopoulos, S.V., Brown, N., Ynchausti, C., Howell, L., Magleby, S.: An origami-inspired foldable reflectarray on a straight-major square-twist pattern. In: 2021 IEEE 21st Annual Wireless and Microwave Technology Conference (WAMICON), pp. 1–4 (2021). IEEE
- [40] Hull, T.: The Augmented Square Twist. <http://origametry.net/ast/ast.html> Accessed 2018-09-13